Chapter 3

CYCLIC OXIDATION BEHAVIOR OF THE SUPER AUSTENITIC STAINLESS STEEL 904L IN AIR AT 500-650 ˚C

CHAPTER - 3

CYCLIC OXIDATION BEHAVIOR OF THE SUPER AUSTENITIC STAINLESS STEEL 904L IN AIR AT 500-650 ˚C

3.1 INTRODUCTION

Earlier studies on majority of SASS have focused mainly on high-temperature deformation/precipitation behavior between 650 to 1000 °C [59]. The 904L steel is a SASS, designed for an intermediate level of oxidation and corrosion resistance up to 480 °C [60]. It contains a high level of Cr and Ni, in addition to Mo and Cu which provide corrosion resistance in certain media. 904L steel is used widely in situations where corrosion resistance of the AISI 317L and 316L stainless steels is not up to the mark [61-63]. Some major uses of the SASS 904L include; wiring in electrostatic precipitators, oil refinery components, gas scrubbing plants, seawater cooling devices, pulp, and paper processing industries, sulphuric, phosphoric and acetic acid processing plants owing to its good corrosion resistance, excellent stability, high strength, and weldability [64]. The standard heat treatment of SASS 904L is solution treatment at 1050-1150 °C and water quenching.

Cao and Norell [48] compared oxidation behavior of 304L and 904L stainless steels in humid air over the temperature range 450-600 °C and observed that oxidation resistance of the 904L was much higher than that of 304L. However, when the nitrogen content of the two steels was increased to a higher level of 10–20 (at.%) through plasma nitriding, there was a reverse trend in oxidation resistance of the two steels. Oxidation resistance in humid air in the temperature range of 450 to 600 °C, under isothermal condition up to 168 h, was

found to be lower for the 904L steel as compared with that of the 304L, due to short range ordering between chromium and nitrogen atoms and less availability of free chromium to form protective oxide of Cr_2O_3. This study was carried out to evaluate their applicability as automobile exhaust, however, for such applications it is more rational to evaluate oxidation resistance against cyclic oxidation rather under isothermal condition.

No report was available on cyclic oxidation behavior of the SASS 904L in air from 500-650°C in open literature. This chapter describes oxidation kinetics of this steel under thermal cycling and characterizing the morphology of the oxidized samples exposed for 100 h at four different temperatures of 500, 550, 600 and 650 °C in still air. The details of experimental procedures are given in the section 2.2 of Chapter 2.

3.2. RESULTS

3.2.1 OXIDATION KINETICS

Oxidation kinetics of the SASS 904L is shown in **Figure 3.1** by plots of weight gain per unit area *(ΔW) vs.* time of exposure (*t*) for 100 h at 500, 550, 600 and 650 ºC in 15 cycles, in still air. After a rapid linear increase in *ΔW* in the beginning, a nearly parabolic behavior was observed, indicating good oxidation resistance of this steel. The relationship between *ΔW* and *t* is shown in equation 3.1.

$$(\Delta W)^2 = k_p t + C \quad \text{----------(3.1)}$$

Where *ΔW* is weight gain per unit area (mg/cm^2), k_p is parabolic rate constant in $mg^2 \cdot cm^{-4} \cdot h^{-1}$, *t* is oxidation time in h and *C* is a constant.

It is evident from **Figure 3.1** that there was highest weight gain in the sample exposed at 650 ºC for 100 h. The values of k_p corresponding to different temperatures of exposure are presented in **Table 3.1**. *ΔW* progressively increased at increasing rate, with rise in temperature of exposure from 500 to 650 ºC. The data points of weight gain corresponding to different temperatures of exposure appear to fall along one line during the initial stage of exposure of 5 h (**Figure 3.1**). However, the insert in **Figure 3.1** at magnified scale reveals increasing slope of *ΔW vs t* plot with increase in temperature, showing higher rate of weight gain at higher temperatures. The rate of weight gain, however, slowly decreased after the initial period of exposure and became lowest after ≈35 h of exposure. **Figure 3.2** shows two distinct segments of high and low slopes in the plots of $(\Delta W)^2$ *vs t* and indicates fast and slow growth behavior of the oxide layer in the initial and later stage of exposure.

Table 3.1: Parabolic rate constant of the SASS 904L oxidized at 500-650 °C up to 100 h.

Temperature (˚C)	ΔW (mg)	Time (h)	k_p ($mg^2 \cdot cm^{-4} \cdot h^{-1}$)	R^2
500	0.3	0-5	0.03	0.9
	0.6	5-100	0.01	0.97
550	0.7	0-5	0.11	0.94
	0.5	5-100	0.01	0.95
600	1.1	0-10	0.13	0.96
	0.4	10-100	0.01	0.9
650	1.9	0-25	0.17	0.98
	0.2	25-100	0.01	0.96

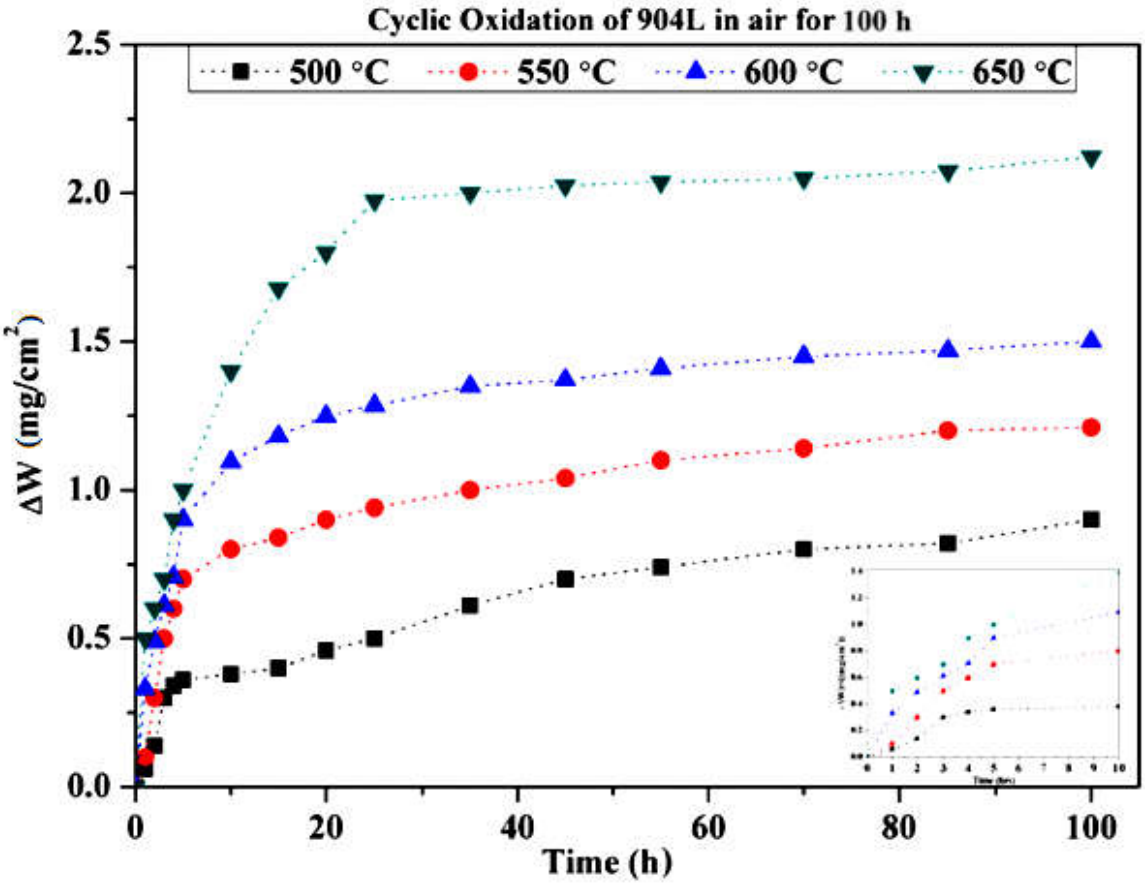

Figure 3.1: Weight change per unit area (ΔW) during oxidation of the SASS 904L in air at 500, 550, 600 and 650 °C up to 100 h.

Table 3.2: Oxide phases formed on the SASS 904L from exposure at 500-650°C for 100 h in air.

Temperature	Phases
500 ˚C	γ-Fe, Cr_2O_3
550 ˚C	Cr_2O_3, Fe_2O_3/Fe_3O_4
600 ˚C	Cr_2O_3, Fe_2O_3/Fe_3O_4, NiO, $NiCr_2O_4$, $FeNi_2O_4$, $(Cr,Fe)_2O_3$
650 ˚C	Cr_2O_3, Fe_2O_3, Fe_3O_4, $FeCr_2O_4$, $NiCr_2O_4$, $FeNi_2O_4$, $(Cr,Fe)_2O_3$

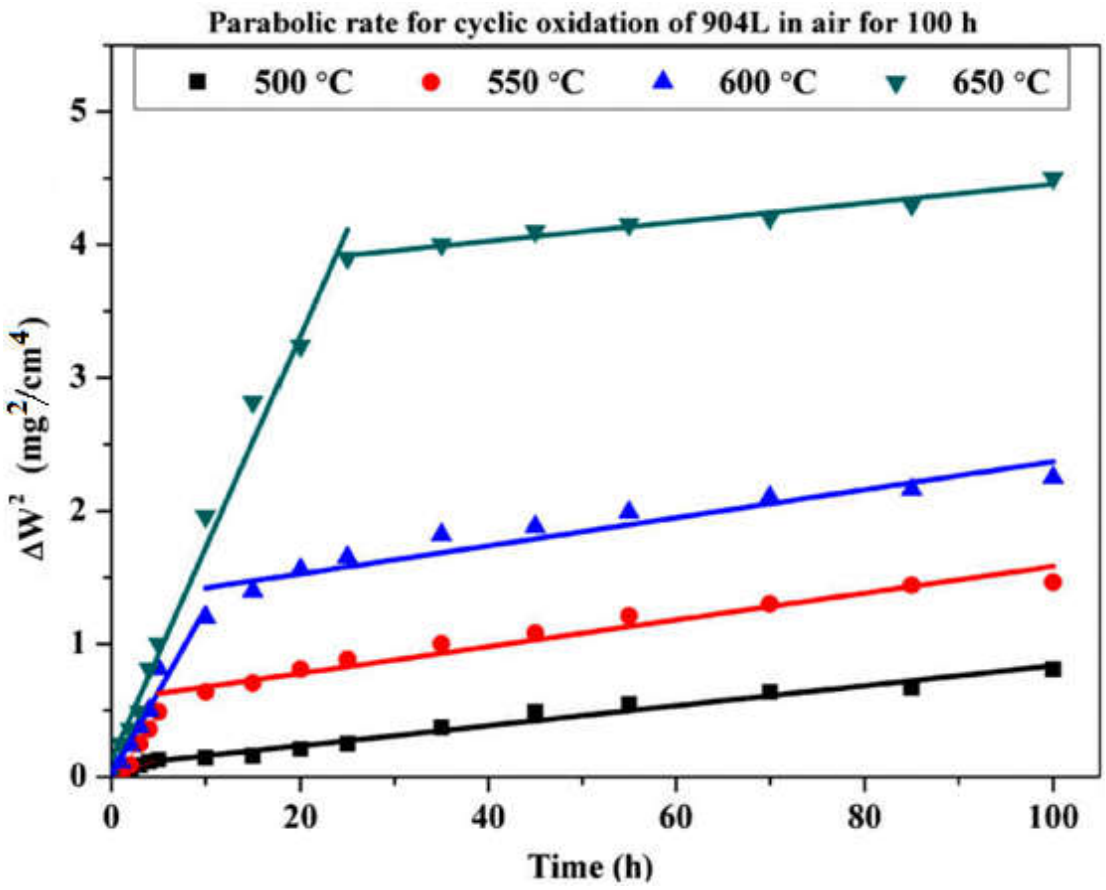

Figure 3.2: Variation of square of weight gain per unit area $(\Delta W)^2$ with time from oxidation of the SASS 904L in air at 500, 550, 600 and 650 °C, up to 100 h.

Based on the values mentioned in **Table 3.1**, plot of $\ln k_p$ versus 1/T is generated for initial 25 hours of cyclically oxidized samples exposed at 500-650 °C, as shown in **Figure 3.3**. The plot showed low activation energy of 76 kJ.

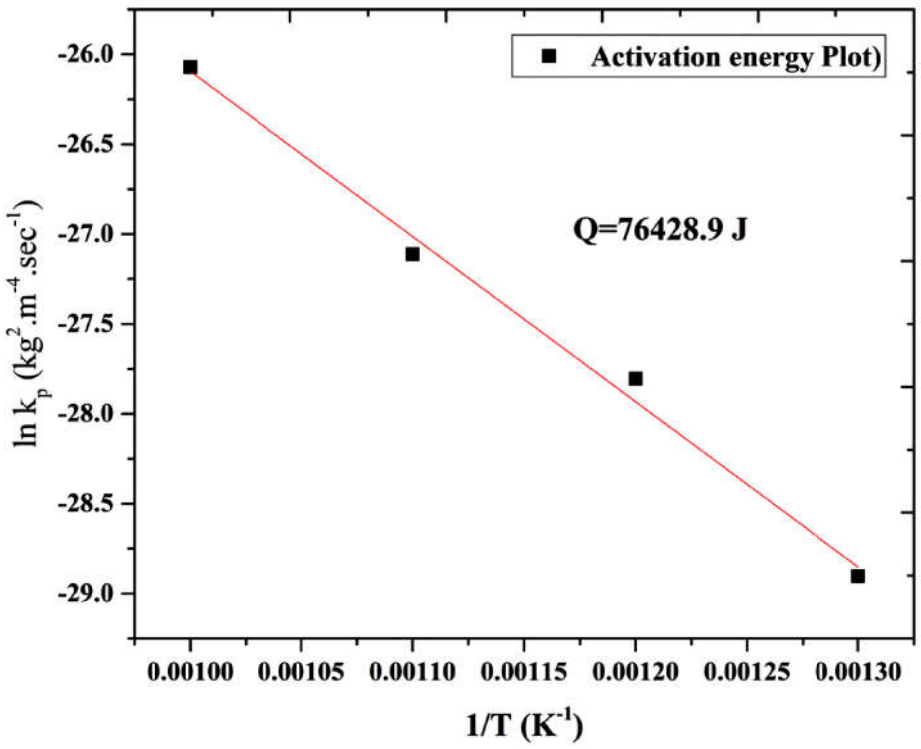

Figure 3.3: Activation energy plot (k_p vs 1/T) for the 1st stage (upto 25 h) cyclic oxidation from 500-650 °C.

3.2.2 PHASE ANALYSIS

X-ray diffraction patterns of the as solution treated sample and those exposed at different temperatures of 500-650 ºC are shown in **Figure 3.4**. The XRD pattern of the as solution treated sample shows standard peaks of only the austenite (γ) phase (**Figure 3.4a**) whereas of that exposed at 500 ºC for 100 h shows also peaks of Cr_2O_3 in addition to peaks of austenite (**Figure 3.4b**) and peaks of Fe_2O_3/Fe_3O_4 along with those of austenite (γ) and Cr_2O_3 in the sample exposed at 550 ˚C (**Figure 3.4c)**. The samples exposed at 600 and 650 ºC show peaks of austenite (γ), iron oxides (Fe_2O_3 and Fe_3O_4), chromium oxide (Cr_2O_3), nickel oxide (NiO) and spinels (**Figures 3.4d and 3.4e**). The various phases revealed by XRD in the different conditions are listed in **Table 3.2**.

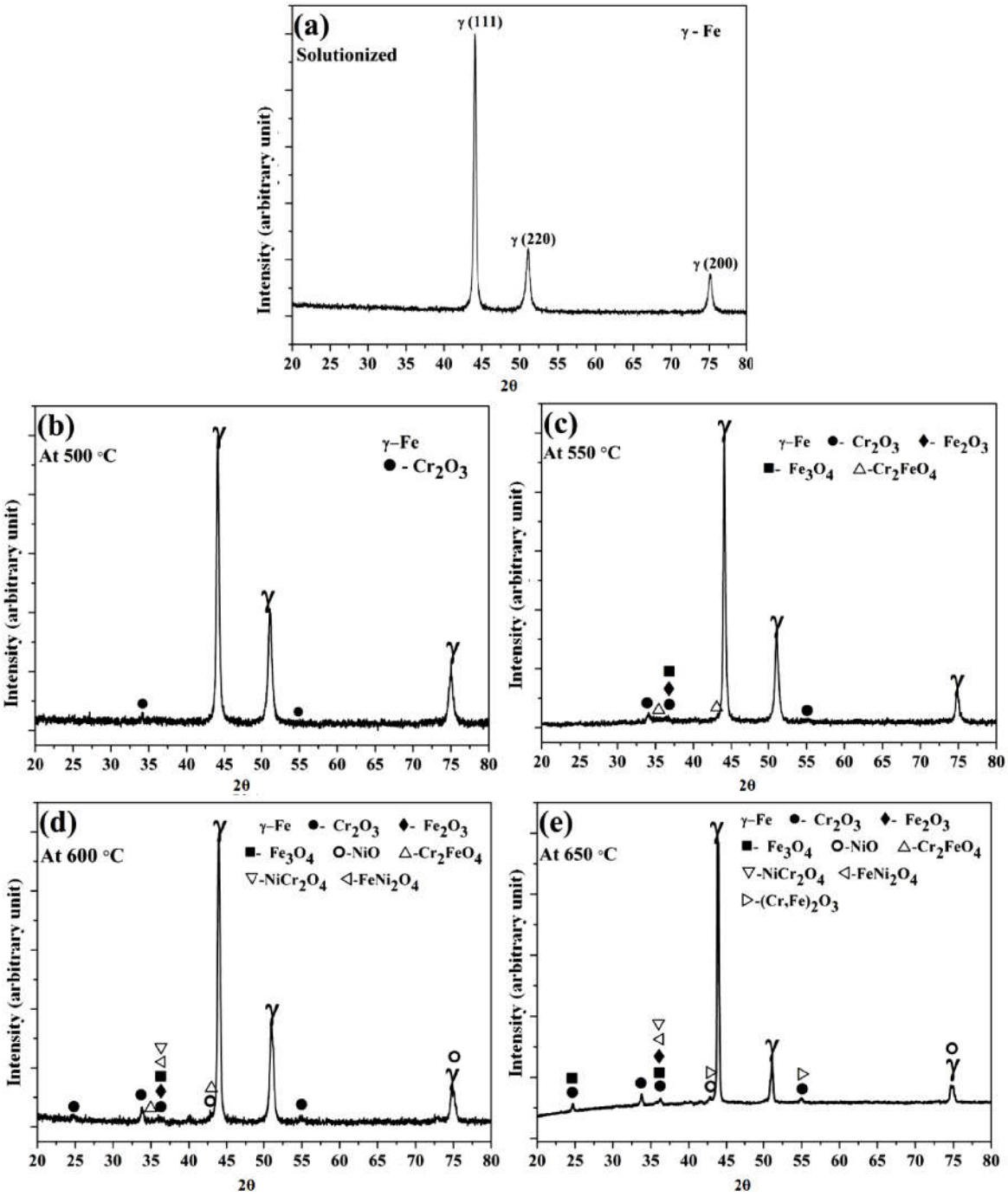

Figure 3.4: XRD patterns of the SASS 904L, (a) in solution treated condition; following oxidation for 100 h at: (b)500, (c)550, (d)600 and (e)650 °C.

3.2.3 SURFACE MORPHOLOGY

Surface morphologies of the different samples revealed by SEM-EDS provide important information related to the process of oxidation. **Figure 3.5(a-d)** shows SEM-EDS of the samples oxidized at 500 to 650 ºC, up to 100 h. There is very thin layer of oxide on the surface of the specimen exposed at 500 °C (**Figure 3.5a**), the crests and trough resulting from mechanical polishing are quite distinct. The thickness as well as roughness of the

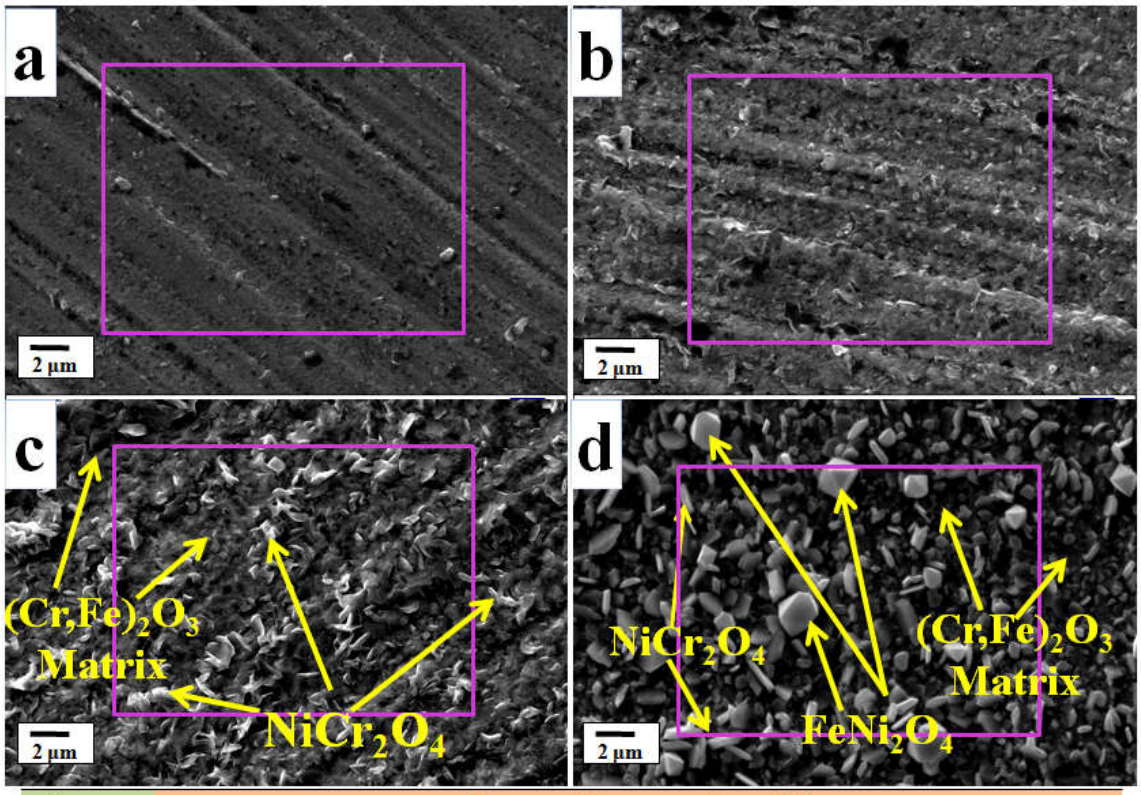

Temp. (˚C)	Compositions are in wt%							
	Mn	Mo	Cr	Ni	Fe	Si	Cu	O
500	0.42	2.22	18.6	21.94	47.26	1.18	1.05	7.31
550	1.69		18.59	20.63	36.87		1.1	21.1
600	1.81	3.65	18.98	14.96	35.01	0.72	2.09	22.77
650	1.88	5.23	22.87	13.49	31	0.97	0.99	23.56

Figure 3.5: Surface morphologies of the samples oxidized for 100 h at different temperatures: (a)500, (b)550, (c)600 and (d)650 °C. Compositional analysis by EDS was carried out from the rectangular enclosed regions.

surface progressively increases with rise in temperature of exposure from 500 to 650 ºC and also there are particles of increasing size (**Figure 3.5 b,c,d**).

There are coarse particles of typical geometrical shapes on the surface of the specimen exposed at 650 ºC (**Figure 3.5d**). The various spinels in the matrix are shown in **Figure 3.5c and 3.5d**. The composition of matrix at the surfaces, exposed at different temperatures, are tabulated below the SEM micrograph, by EDS analysis of the rectangular enclosed regions. It is relevant to mention that there was no spalling of the surface exposed at 500 to 650 ºC.

3.2.4 CROSS SECTIONAL STUDY BY SEM (EDS)

Figure 3.6(a-d) shows secondary electron image (SE) of the samples exposed at 500, 550, 600 and 650 ºC respectively, with contents of the different elements at marked locations. It may be seen that there is progressive increase in the thickness of the oxidized layer.

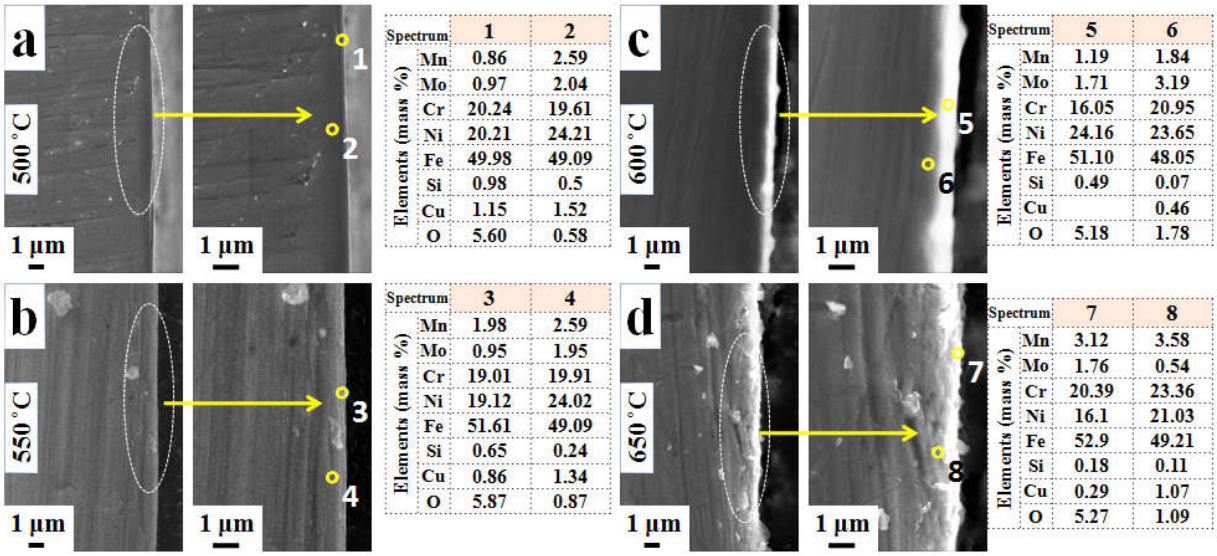

Spectrum	1	2
Mn	0.86	2.59
Mo	0.97	2.04
Cr	20.24	19.61
Ni	20.21	24.21
Fe	49.98	49.09
Si	0.98	0.5
Cu	1.15	1.52
O	5.60	0.58

Elements (mass %)

Spectrum	3	4
Mn	1.98	2.59
Mo	0.95	1.95
Cr	19.01	19.91
Ni	19.12	24.02
Fe	51.61	49.09
Si	0.65	0.24
Cu	0.86	1.34
O	5.87	0.87

Elements (mass %)

Spectrum	5	6
Mn	1.19	1.84
Mo	1.71	3.19
Cr	16.05	20.95
Ni	24.16	23.65
Fe	51.10	48.05
Si	0.49	0.07
Cu		0.46
O	5.18	1.78

Elements (mass %)

Spectrum	7	8
Mn	3.12	3.58
Mo	1.76	0.54
Cr	20.39	23.36
Ni	16.1	21.03
Fe	52.9	49.21
Si	0.18	0.11
Cu	0.29	1.07
O	5.27	1.09

Elements (mass %)

Figure 3.6: Cross-sectional SEM-EDS of the samples oxidized at different temperatures: (a)500, (b)550, (c) 600 and (d)650 °C for 100 h.

3.2.5 EPMA MAPPING OF THE CROSS-SECTION

EPMA analysis of cross sections of the samples exposed from 500-650 ºC for 100 h is shown in **Figure 3.7**. There is progressive but heterogeneous enrichment of oxygen on surface of the specimens exposed from 500-650 ºC. Also, there is heterogeneous enrichment of iron on the surface of the samples exposed from 550-650 ºC. There was enrichment of chromium, covering entire surface of the specimens, exposed at 500-650 ºC, without any discontinuity. The thickness of the enriched chromium layer increases with the

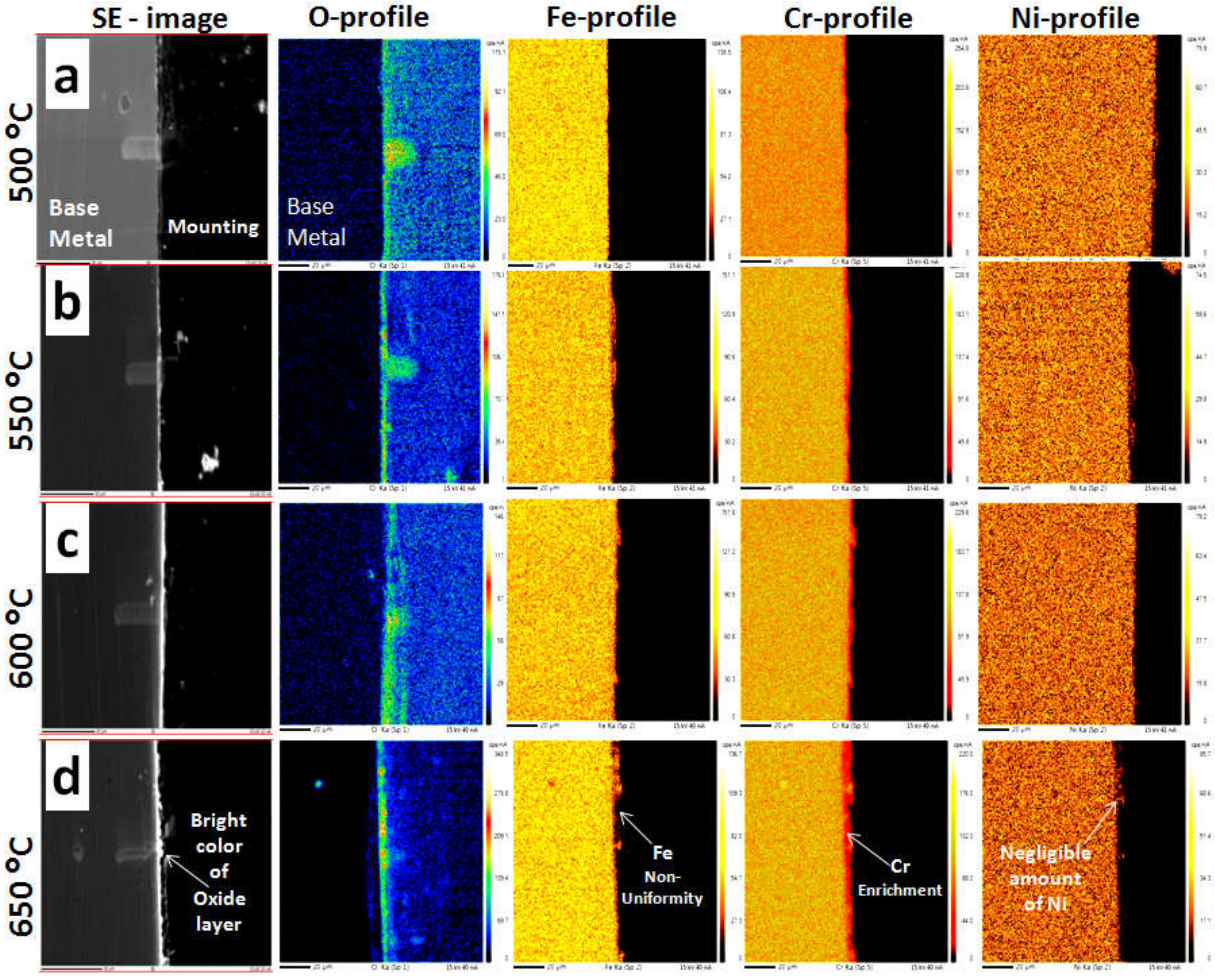

Figure 3.7: EPMA analysis of cross-sections of the samples exposed at 500 to 650 °C up to 100 h.

temperature of exposure, however, uniformity of the outer surface of the enriched layer decreases with increase in the temperature of exposure. There is very less enrichment of nickel, only on surface of the specimen exposed at the highest temperature of 650 ˚C (**Figure 3.7d**).

3.3. DISCUSSION

This investigation clearly reveals that in the intermediate-range of temperatures, from 500 to 650 °C, there is rapid weight gain in the initial stage of exposure, with increasing rate as well as in amount, with increase in temperature from 500-650 °C, in ambient air. The kinetics of oxidation exhibits parabolic rate law with high and low parabolic rate constants, corresponding to the initial and later stage of exposure, due to difference in the kinetics of oxidation and the rate of diffusion of metal cations from interior to surface **(Table 3.1)**. The process of oxidation starts with interaction of metal cations and oxygen anions at interface of the material and air and leads to formation of their oxides on surface of the material [65]. Based on the earlier work on chromium containing iron alloys, on the proportion of formed oxides of chromium and iron, it was observed that the formation of chromium oxides is thermodynamically favored while that of iron oxides is kinetically controlled [66]. Since oxidation temperature and oxygen exposure are known to be the two key factors for the rate of oxidation, surface composition and type of oxides [67, 68], the higher rate and amount of weight gain in the initial stage of exposure, at increasing temperatures may thus be understood. The proportion of the formed oxides in the beginning would also be affected by bulk diffusion coefficients of the different metal cations through austenitic matrix of the 904L steel. It has been established in the austenitic

Fe-20Cr-12Ni-Si alloy that at elevated temperature (800-1400 °C) $D_{Cr}>D_{Fe}>D_{Ni}$ [69]. The same trend was found at 500-650 °C, from extrapolation of the high temperature data of Rothmann et. al., [69]. It is presumed that a similar trend would have been also in the austenitic 904L steel. It may be seen from the XRD patterns (**Figure 3.4**) that there is formation of only Cr_2O_3 which appears to be very thin at 500 °C (**Figures 3.5 and 3.6**), likewise there is very little weight gain (**Figure 3.1**), whereas at 550 °C there is formation of Fe_2O_3, Cr_2O_3 and spinels of Fe_2O_3-Cr_2O_3. At 600 and 650 ˚C there is formation of additional spinels of different oxides along with Cr_2O_3 and Fe_2O_3. There is relatively fast growth rate of kinetically controlled iron containing oxides, resulting from rapid oxidation in the early stage. However, subsequent selective oxidation of chromium and formation of Cr_2O_3 because of most negative ΔG value of its formation (**Table 3.3**) leads to formation of a healing Cr_2O_3 layer at the base of the previously formed oxides and spinels, and the further rate of oxidation is drastically reduced due to its strong barrier action. The scales were found intact and there was no spalling. Further, there was no sign of internal oxidation, therefore the process of oxidation was controlled by diffusion of metal cations to outer surface of the scale. Once there is formation of uniform layer of Cr_2O_3, further process of oxidation is drastically reduced because it is controlled by the rate of diffusion of metal cations through the layer of the protective Cr_2O_3. It has been established earlier that $D_{Cr}>D_{Fe}>D_{Ni}$ in the Cr_2O_3 layer [51, 70, 71]. Since, Cr content in the 904L steel is more than the critical content of 18 wt% [57, 72] for the formation of continuous and protective layer of Cr_2O_3, this material remains resistant to oxidation from 500-650 ˚C. Due to relatively higher diffusivity of Cr cations and their adequate supply from the substrate there was slow but continued growth of Cr_2O_3, hence the negative effect of lower

resistance of spinel of oxides against diffusion of metals cations through them was counteracted. It may further be noted from the distribution of the different elements in the scale (**Figure 3.7**) that the content of other elements as compared to Cr is much less, hence their deleterious effect as spinels of their oxides, in promoting diffusion of cations through them was less, even in the later stage of exposure, at least up to 100 h of exposure, observed in the present investigation. The non-uniformity in the thickness of the scale may be attributed to dissimilarity in orientations of the coarse grains of 40 micron mean intercept length. It may be seen in **Figure 3.2** that there is dual slope of high and low inclination corresponding to initial and later stage of exposure. This behavior is from rapid weight gain in the initial stage due to fast diffusion of Cr, Fe and Ni through the austenite matrix to surface and formation of their oxides. However, in the later stage the rate of weight gain is reduced due to much slower diffusion of these elements through the protective oxide layer of Cr_2O_3 formed on the surface. This observed behavior of dual slope in the present investigation is in line with the earlier investigation made on Sanicro-25 which is very close in composition to the 904L steel [73-76]. The composition of Sanicro-25 may be seen to be very close to that of 904L, the material of present investigation (**Table 3.1**). The faster rate of weight gain in the initial stage may also be assisted by the relatively higher potential of oxygen, from more frequent opening of the furnace in the initial thermal cycles, as compared to later stage cycles of much longer durations.

It may be seen from **Figure 3.4** that there are strong peaks of γ-phase from all the exposed samples, including the one exposed at the highest temperature at 650 °C. Thus, it

is obvious that oxide scales were too thin to stop penetration of X-rays through them to austenite substrate, and all the phases formed from oxidation were exposed to X-rays.

Table 3.3: Standard Gibbs free energy of formation of different oxides.

ΔG (in kJ/mole)	**Fe_2O_3**	**Fe_3O_4**	**Cr_2O_3**	**$FeCr_2O_4$**	**NiO**	MnO
ΔG_{500}	-140.72	-215.51	-919.42	-472.35	-168.46	-77.40
ΔG_{550}	-133.68	-209.25	-906.43	-467.28	-164.20	-73.76
ΔG_{600}	-126.65	-203.00	-893.44	-462.22	-159.94	-70.12
ΔG_{650}	-119.62	-196.74	-880.45	-457.16	-155.68	-66.48

3.3.1 OXIDATION MECHANISM

The mechanism of oxidation of the SASS 904L at different temperatures is shown schematically **in Figure 3.8**. At 500 °C, Cr forms a thin layer of Cr_2O_3 due to high affinity of Cr with O_2 (**Figure 3.8**). With rise in the temperature, at 550 °C (**Figure 3.8b**), Cr_2O_3 layer grows and a layer of iron oxide also forms. This shows a matrix with lean presence of Fe-Cr and Ni-Cr oxide spinel, confirmed by XRD and SEM surface analysis. At 600 °C (**Figure 3.8c**), the dark appearance of the layer shows Fe enrichment over the Cr oxide matrix. In addition to these enrichments the growth of oxide particles through the matrix occurs which were rich in Fe, Ni and Cr oxides. At 650 °C, (**Figure 3.8d**) the enriched Fe and Cr combined to form corundum type of oxide $(Fe,Cr)_2O_3$ and further growth of spinel oxides such as of Ni-Cr and Fe-Ni took place.

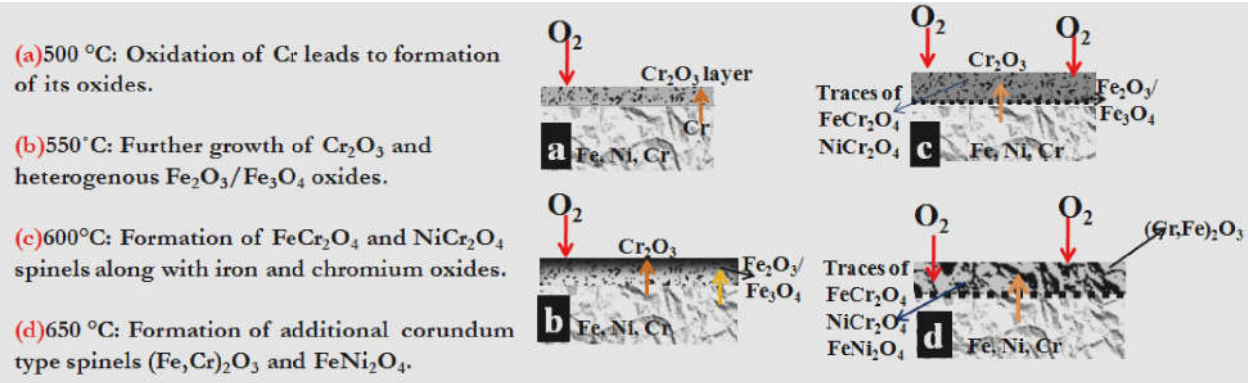

Figure 3.8: Schematic process of oxidation of the SASS 904L from 100 h of exposure at different temperatures: (a)500, (b)550, (c)600 and (d)650 °C.

3.4 CONCLUSION

1. The rate as well as the amount of weight gain per unit area (ΔW) was high under the cyclic oxidation, during the initial stage of oxidation and increased with rise in temperature from 500-650 ˚C.
2. Parabolic rate law was exhibited, however, there was dual slope in the plot of ΔW^2 *vs* t, with higher and lower values of kp, corresponding to the initial and later stage of exposure. The oxidation kinetics was temperature dependent and fast during the initial 25h, as expected from the observed low activation energy for oxidation. In the later stage oxidation rate was slower due to formation of adherent passive layer.
3. While there was formation of Cr_2O_3 at 500 ˚C and Cr_2O_3, Fe_2O_3/Fe_3O_4 at 550 ˚C, also there was formation of different spinels of oxides at 600 and 650 ˚C apart from the chromium and iron oxides.
4. A mechanism of oxidation is proposed based on the morphology of the different phases and EPMA analysis of the cross sections of the oxidized samples.